Supplement to Path-Dependent Supercooling of the ^{3}He Superfluid A-B transition*

Dmytro Lotnyk[1], Anna Eyal[1,2], Nikolay Zhelev[1], Abhilash Sebastian[1,3], Yefan Tian[1], Aldo Chavez[1], Eric Smith[1], John Saunders[4], Erich Mueller[1] and Jeevak Parpia[1]

[1]*Department of Physics, Cornell University, Ithaca, NY, 14853 USA*

[2]*Physics Department, Technion, Haifa, Israel*

[3]*VTT Technical Research Centre of Finland Ltd, Espoo, Finland and*

[4]*Department of Physics, Royal Holloway University of London, Egham, TW20 0EX, Surrey, UK*

(Dated: June 3, 2021)

* Corresponding Author: Jeevak Parpia: jmp9@cornell.edu

SUPPLEMENTARY NOTE 1. COMPARISON TO EARLIER EXPERIMENTS

Previous experiments observing supercooling [1–5] were performed in a variety of magnetic fields (that favors the A phase over the B phase and extends supercooling). The experiments in Ref [5] that display exceptionally strong supercooling were carried out with smooth surfaces with well characterized roughness and isolated from the rest of the fluid by means of a magnetic "valve" that ensured that B phase external to the sample under study could not initiate an A→B transition. In comparison, the other experiments cited were performed in containers with rougher surfaces, and in some cases with sinter or powders in contact with the ^{3}He sample under study. Thus they are not immediately applicable to our results. With the exception of the experiments in [1], none of the experiments focused on the polycritical point. No experiment changed the pressure after traversing T_c in the course of a cool down.

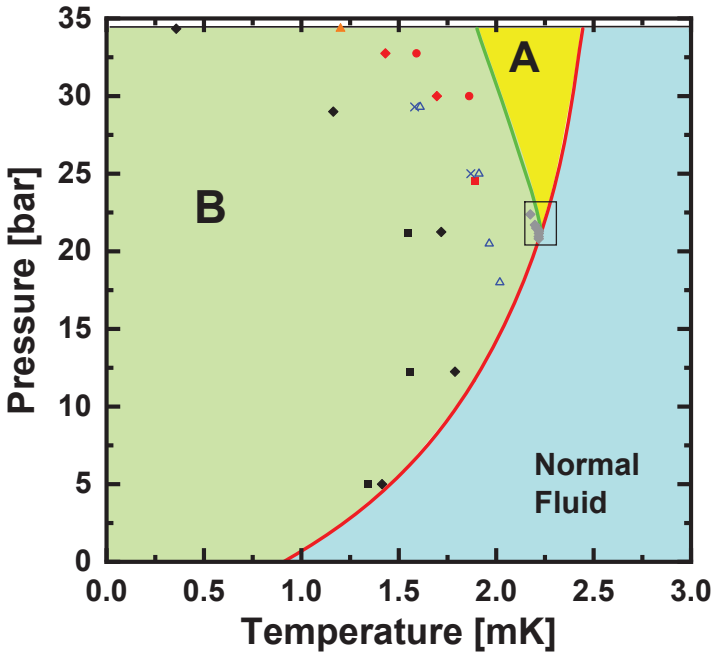

Supplementary Figure 1. The phase diagram of ^{3}He [6, 7], showing the extent of the equilibrium A phase (yellow), the B phase (green) separated by the equilibrium T_{AB} line (green). Superfluidity onsets at the T_c line (red). The region investigated here is within the box centered on the polycritical point. Previous supercooling measurements performed in various magnetic fields are shown with symbols: (⧫, 4.9 mT, 0.5 mT [1]; ×, 56.9 mT; △, 28.4 mT [2]; ▲, 0 mT [3]; ●, 0 mT; ⧫, 10.0 mT; ■, 20.0 mT [4]; ■, ⧫, 28.2 mT [5].

SUPPLEMENTARY NOTE 2. EXPERIMENTAL DETAILS

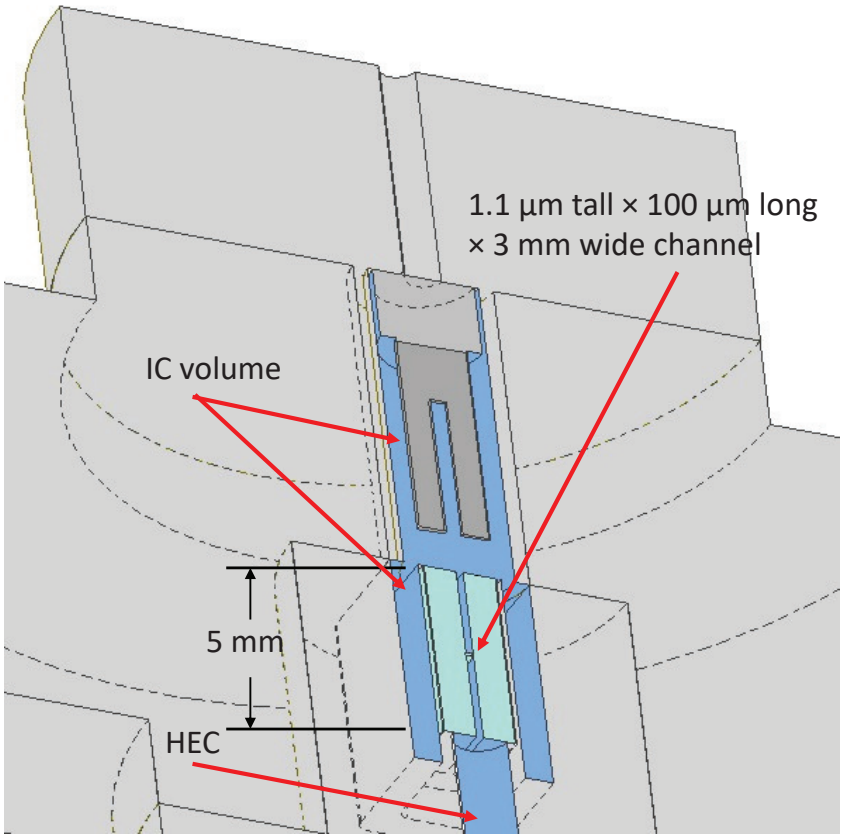

Supplementary Figure 2. Schematic of the IC. The assembly comprising the silicon and glass channel is shown as light blue and is 5 mm in length. The channel separating the IC (top) and HEC (region below the channel) is in the form of a wide septum with a letterbox shape 100 μm long $\times$ 1.1 μm tall $\times$ 3 mm wide, and is shown in cross-section with the channel width not visible here. Most of the open volume resides in the bulk liquid surrounding the channel holder and around the quartz fork located above the channel. There are regions where close fitting coin-silver components that comprise the cell structure are separated by gaps of order 25 μm that may promote the A phase. All surfaces of the coin-silver components are as-machined metal.

The measurement of the A$\rightarrow$B transition occurs in a small volume isolated chamber (IC) connected to a chamber containing a heat exchanger (HEC) through a 1.1 μm high, 3 mm wide, and 100 μm long channel with 200 μm tall $\times$ 3 mm wide $\times$ 2.45 mm long "lead-in" sections at either end. The 1.1 μm height section should be filled with the A phase at all temperatures and pressures explored in this paper. The arrangement is illustrated in Fig. 1

(b) of the main paper. The channel (Supplementary Figure 2) was nanofabricated in 1 mm thick silicon, capped with 1 mm thick sodium doped glass, anodically bonded to the silicon[8] and then glued into a coin silver carrier. In the mK temperature regime, the IC was cooled through the A-phase-filled channel with a thermal time constant ∼1500 s at the superfluid transition temperature, T_c, limiting the cooling rate achievable in the experiment[9].

The volume of the IC is estimated to be 0.14 ± 0.02 cm^3, and the area of all wetted surfaces in the IC was estimated to be 14.5 ± 0.5 cm^2. In comparison, the HEC had a volume of 0.72 ± 0.1 cm^3 and a surface area of 3.5 ± 0.5 m^2 due to the heat exchanger.

SUPPLEMENTARY NOTE 3. PRESSURE DIFFERENCE ACROSS CHANNEL, POWER DISSIPATED, HEAT LOAD AND THERMAL GRADIENTS WHILE RAMPING PRESSURE.

We estimate the pressure difference across the channel that must accompany the pressurization or depressurization of the ^{3}He in the system. We start with the equation that links pressure, impedance, viscosity and flow:

$$\Delta P = Z\eta \; dV/dt, \tag{1}$$

where ΔP [Pa] is the pressure across the channel, Z [m^{-3}] is the impedance, η [kg m^{-1} s^{-1}] is the viscosity of the ^{3}He at T_c, and dV/dt [m^3 s^{-1}] is the flow rate through the channel accompanying a change in pressure of the system. The impedance for a rectangular channel, $Z = 12\; l/wd^3$ is defined by its length $l = 100$ μm, width $w = 3$ mm, and height $d = 1.1$ μm, resulting in $Z = 3{\times}10^{17}$ m^{-3}. The viscosity of the system is largest at T_c and is estimated to be 0.02 kg m^{-1} s^{-1} [10] in bulk ^{3}He. In the channel, owing to confinement, the normal fluid is subject to slip and the effective viscosity is given by $\eta_{\rm EFF} = s \times \eta$, with the slip factor, s, dependent on the Knudsen number (K_n). $K_n = \lambda_\eta/d$, where λ_η is the viscous mean free path. A simplified upper bound for the correction factor s is given by $s = 1/(1 + 2K_n)$. With the mean free path of order 1 μm at T_c, $K_n \approx 1$. Thus s is ≈1/3, reducing the effective viscosity to 0.007 kg m^{-1} s^{-1} at T_c. Below T_c, the normal viscosity decreases by a further factor of 3[10, 11], and in the superfluid state the effective viscosity of the normal fluid just below T_c, $\eta_n(0.99T_c) \approx 0.002$ kg m^{-1} s^{-1}. Our maximum pressurization or depressurization rate was 1.3 bar/day.

To estimate dV/dt we require the molar volume $V_{\rm m} = 27.36{\times}10^{-6}$ m^3 mole^{-1} and d$V_{\rm m}$/dP = -0.185 $\times 10^{-6}$ m^3 mole^{-1} bar $^{-1}$ [6]. The flow rate can be computed by multiplying the molar volume $V_{\rm m}$ by the molar flow rate, dn/dt

$$dV/dt = V_{\rm m} \times dn/dt, \tag{2}$$

and dn/dt can be calculated from the equation

$$dn/dt = -V_{\rm IC}/V_{\rm m}^2 \times dV_{\rm m}/dP \times dP/dt. \tag{3}$$

The volume of the isolated chamber, $V_{\rm IC} = 0.14{\times}10^{-6}$ m^3; we estimate dV/dt= $1.4{\times}10^{-14}$ m^3 s^{-1}.

Thus, the expected magnitude of the pressure drop across the channel at the maximum pressurization or depressurization rate is 8 Pa or $\sim$ 0.1 mbar, below the superfluid transition. The impedance of the fill line (filled with normal fluid, with a 100 μm diameter and thus not subject to slip) below mixing chamber temperatures is of order 10^{17} m^{-3}. The volume rate of flow is estimated to be of order $1{\times}10^{-13}$ m^3 s^{-1} (due to to combined volumes of HEC and IC). Since the viscosity varies as T^{-2}, the pressure drop would mainly occur at the low temperature end of the fill line. We estimate a pressure drop of no more than 10 times that across the channel in the fill line. Above that temperature, the lower viscosity of the ^{3}He implies negligible pressure differences due to pressurization rates. The hydrostatic pressure difference due to the density differences in the liquid (at cryogenic temperatures) and the gas at room temperature is of order 15 mbar, but this is present whether the cell is operated at constant pressure or while being pressurized. In summary, the pressure in the IC while pressurizing or depressurizing is not significantly different from that at the room temperature controller.

We can also estimate the power dissipated in the channel on account of viscous heating due to flow while changing the pressure when the experiment is below $T_{\rm c}$. The power can be expressed as the product of the pressure difference across the channel, ΔP (Supplementary Eq. 1) multiplied by the volume flow rate, dV/dt (Supplementary Eq. 2) (and thus varies as the square of the flow rate). The power, dQ/dt is found to be 8 Pa $\times$ $1.4{\times}10^{-14}$ m^3 s^{-1} $\approx 10^{-13}$ W. This power dissipation would lead to a thermal gradient $\Delta T = dQ/dt{\times}\ R_{\rm TH}$, where $R_{\rm TH}$ is the thermal resistance of the channel = $1.5{\times}10^6$ K/W[9]. Thus we estimate at our maximum pressurization/depressurization rate, a thermal offset of order 10^{-13} W $\times$

1.5×10^6 K/W = 0.15 μK would appear across the channel. This temperature difference is too small to measure.

The temperature rise due to the addition of ^{3}He thermalized at the mixing chamber temperature into the HEC on account of the pressurization can also be estimated. The volume of the HEC and IC combined is estimated to be 0.86×10^{-6} m^3[9]; we write the total flow into the cell as dV/dt= 8.6×10^{-14} m^3 s^{-1}, and taking into account the molar volume of the ^{3}He at 22 bar as $V_{\rm m} = 27.36\times10^{-6}$ m^3/mole, the inflow of ^{3}He (dn/dT) is estimated to be 3.14×10^{-9} moles/s.

The molar specific heat in the normal state is γnRT[6], with R = 8.314 J/mole K, T the temperature in K, and $\gamma \approx 4$. In the superfluid, we assume that the specific heat follows a T^3 behavior after a discontinuous increase by a factor of 3 at the superfluid transition. We further assume that the heat load is calculated at a temperature of $0.95T_{\rm c}$, close to the lowest temperature for measurements discussed here at the polycritical point. The heat load dQ/dt due to the influx of ^{3}He at mixing chamber temperature ($T_{\rm H}$ = 10 mK) to the superfluid transition temperature ($T_{\rm c}$ = 2.273 mK) and then from $T_{\rm c}$ to $0.95T_{\rm c}$ is given by

$$dQ/dt = dn/dt \times \left[\int_{T_{\rm c}}^{T_{\rm H}} \gamma RT\, dT \; + \int_{0.95T_{\rm c}}^{T_{\rm c}} 3\gamma RT_{\rm c}(T/T_{\rm c})^3\, dT \right], \tag{4}$$

after accounting for the 3$\times$ heat capacity increase at the superfluid transition. This yields a heat load of order 5 pW. The heat exchanger has a surface area A = 3.2 m^2, and using the standard value of Kapitza boundary resistance, $R_{\rm K} = 250\, T^{-1}/A$ (with T in K, A in m^2 [12], we find $R_{\rm K} = 31 \times 10^3$ K/W. We estimate the temperature rise at the heat exchanger due to inflow of ^{3}He to be of order 0.15 μK, again too small to measure. The total additional temperature increase on account of the pressure ramp is $\leq$0.5 μK. Thus the T, P coordinates while ramping the pressure and temperature are not significantly altered from what would be observed while cooling at the same rate at constant pressure. This is consistent with our observation that on stopping the pressure ramp (under conditions of constant cooling rate), no transient cooling was observed implying that the additional heat lead on account of the pressure ramp is negligible.

SUPPLEMENTARY NOTE 4. RELATIONSHIP BETWEEN $T_{\rm PLTS}$, $T_{\rm G}$ AND THE PHASE DIAGRAM OF ^{3}HE.

$P-P_{\rm A}$ (mbar)	$T_{\rm G}$ (mK)	$T_{\rm PLTS}$ (mK)	$P-P_A$ (mbar)	$T_{\rm G}$ (mK)	$T_{\rm PLTS}$ (mK)
52.7	-	0.90944	25	1.78732	1.76047
52	0.94925	0.92816	24	1.81646	1.78881
51	0.98446	0.96438	23	1.84551	1.81704
50	1.01862	0.99938	22	1.87446	1.84518
49	1.05205	1.03349	21	1.90332	1.87322
48	1.08492	1.06691	20.2	-	1.89558
47	1.11738	1.09978	20	1.93209	1.90116
46	1.14949	1.13219	19	1.96078	1.92901
45	1.18134	1.16421	18	1.98938	1.95677
44	1.21295	1.1959	17	2.01789	1.98445
43	1.24436	1.2273	16	2.04633	2.01204
42	1.2756	1.25843	15	2.07468	2.03956
41	1.30668	1.28932	14	2.10295	2.06699
40	1.33761	1.31999	13	2.13115	2.09435
39	1.3684	1.35045	12	2.15927	2.12163
38	1.39907	1.38073	11	2.18732	2.14884
37	1.4296	1.41082	10	2.2153	2.17598
36	1.46002	1.44074	9	2.2432	2.20305
35	1.49032	1.4705	8	2.27104	2.23006
34	1.5205	1.5001	7	2.29881	2.257
33	1.55057	1.52955	6	2.32651	2.28388
32	1.58053	1.55886	5	2.35415	2.3107
31	1.61039	1.58804	4	2.38173	2.33746
30	1.64013	1.61708	3	2.40924	2.36416
29	1.66977	1.64599	2	2.4367	2.3908
28	1.69931	1.67479	1	2.46409	2.4174
27	1.72875	1.70346	0	2.49143	2.44393
26	1.75808	1.73202			

TABLE I. $P-P_{\rm A}$ and $T_{\rm G}$, $T_{\rm PLTS}$ from the polynomial functions provided in [6, 7].

Temperatures reported in this work were referenced to a ^{3}He melting curve thermometer. The most recent temperature scale in the mK regime utilizes the melting curve[7], and is designated as $T_{\rm PLTS}$. Unfortunately, $T_{\rm PLTS}$ does not provide a map onto the phase diagram of ^{3}He as measured by Greywall[6]. Fortunately since both the measurements reference pressure relative to the pressure of the superfluid transition at the melting curve $P_{\rm A}$, the temperature scale provided by Greywall, $T_{\rm G}$ and $T_{\rm PLTS}$ are readily mapped onto one another especially in the regime between 2.5 mK and the 0.9 mK. Below we describe the procedure

we used to generate the conversion.

We generate a table of $P - P_{\rm A}$ and $T_{\rm G}$, $T_{\rm PLTS}$ from the polynomials provided in [6, 7], with T in mK and P in bar throughout.

We then plot and fit the two scales over the temperature range between 0.9 and 2.5 mK. Over this limited regime, the two scales can be well fitted by a third order polynomial, with systematic deviations of less than $\pm$ 1 μK. the fit we obtained is

$$T_{\rm PLTS} = -0.1017 + 1.16054 T_{\rm G} - 0.09347 T_{\rm G}^2 + 0.01519 T_{\rm G}^3, \tag{5}$$

and was used to generate the phase diagrams shown in this Letter. Meanwhile, the relation between $P - P_{\rm A}$ and $T_{\rm PLTS}$ is given as $T_{\rm PLTS} = \sum_i a_i (P - P_A)^i$, with $a_0 = 2.44372$, $a_1 = -0.02626$, $a_2 = -8.62695 \times 10^{-5}$, $a_3 = 5.37473 \times 10^{-6}$, $a_4 = -2.4168 \times 10^{-7}$, $a_5 = 4.7687 \times 10^{-9}$, and $a_6 = -3.63205 \times 10^{-11}$. The values of $T_{\rm AB,PLTS}$ and $T_{\rm c,PLTS}$ are listed in the accompanying Tables II, III. In addition, we also provide here $T_{\rm AB,PLTS}$ and $T_{\rm c,PLTS}$ as a polynomial function of pressure, $T_{\rm AB,PLTS} = \sum_i a_i P^i$, with $a_0 = -26.90119$, $a_1 = 5.27149$, $a_2 = -0.37666$, $a_3 = 0.01334$, $a_4 = -2.35395 \times 10^{-4}$, and $a_5 = 1.65395 \times 10^{-6}$; $T_{\rm c,PLTS} = \sum_i a_i P^i$, with $a_0 = 0.90951$, $a_1 = 0.14054$, $a_2 = -0.00742$, $a_3 = 2.87065 \times 10^{-4}$, $a_4 = -6.51355 \times 10^{-6}$, and $a_5 = 6.06738 \times 10^{-8}$.

P (bar)	$T_{{\rm AB},G}$ (mK)	$T_{\rm AB,PLTS}$ (mK)
$P_{\rm AB}$	1.932	1.901
34	1.941	1.910
33	1.969	1.937
32	1.998	1.965
31	2.027	1.993
30	2.056	2.021
29	2.083	2.047
28	2.111	2.075
27	2.137	2.100
26	2.164	2.126
25	2.191	2.152
24	2.217	2.177
23	2.242	2.202
22	2.262	2.221
21.22	2.273	2.232

TABLE II. The equilibrium $T_{\rm AB}$ as a function of Pressure, using $P, T_{\rm AB}$ from Reference [6], and Equation 5 to generate $T_{\rm AB,PLTS}$. $P_{\rm AB}$ specifies the pressure of the equilibrium A-B transition at melting pressure.

P (bar)	$T_{c,G}$ (mK)	$T_{c,PLTS}$ (mK)
34.338	2.491	2.444
34	2.486	2.439
33	2.474	2.427
32	2.463	2.417
31	2.451	2.405
30	2.438	2.392
29	2.425	2.380
28	2.411	2.366
27	2.395	2.350
26	2.378	2.334
25	2.360	2.316
24	2.339	2.296
23	2.317	2.274
22	2.293	2.251
21	2.267	2.226
20	2.239	2.199
19	2.209	2.170
18	2.177	2.139
17	2.143	2.106
16	2.106	2.070
15	2.067	2.032
14	2.026	1.992
13	1.981	1.949
12	1.934	1.903
11	1.883	1.854
10	1.828	1.800
9	1.769	1.743
8	1.705	1.681
7	1.636	1.613
6	1.560	1.539
5	1.478	1.458
4	1.388	1.370
3	1.290	1.272
2	1.181	1.164
1	1.061	1.043
0	0.929	0.908

TABLE III. The Superfluid Transition Temperatures as a function of Pressure, using P, T_c from Reference [6], and Equation 5 to generate $T_{c,PLTS}$.

SUPPLEMENTARY NOTE 5. CONSTANT PRESSURE COOLING RUNS AT THE LOWEST PRESSURES WHERE T_{AB} WAS OBSERVED.

In Supplementary Figure 3 we show the traces of Q *vs* T at 5 closely spaced pressures all taken while cooling slowly at constant pressure. At the lowest pressure 20.88 bar, no A→B transition is seen. At 20.89 bar, the transition is seen well below T_c.

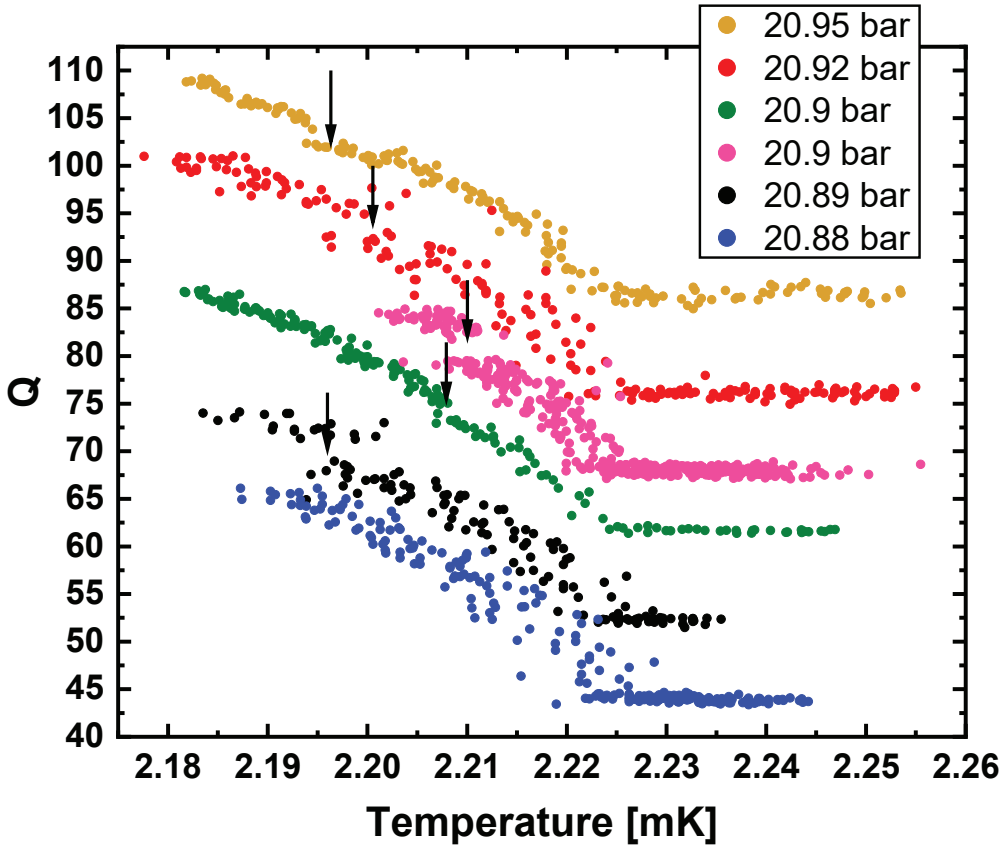

Supplementary Figure 3. Traces of the Q vs temperature for slow cooled transitions at low pressures. The A→B transition is not clearly seen in the pulsed Q *vs.* t traces though slow cooled transitions show A→B transitions. Arrows mark the assigned temperatures for $T_{A\to B}$ (See also Fig. 2, 3 in the main paper, and Supplemental Figs. to follow). Q values for pressures above 20.88 bar each offset by 7 for clarity.

In supplementary Figure 4, we show the distributions of the fast cooled transitions shown in Figure 3 b,c of the main paper along with those seen at an intermediate pressure. The distribution broadens significantly at the lowest pressure.

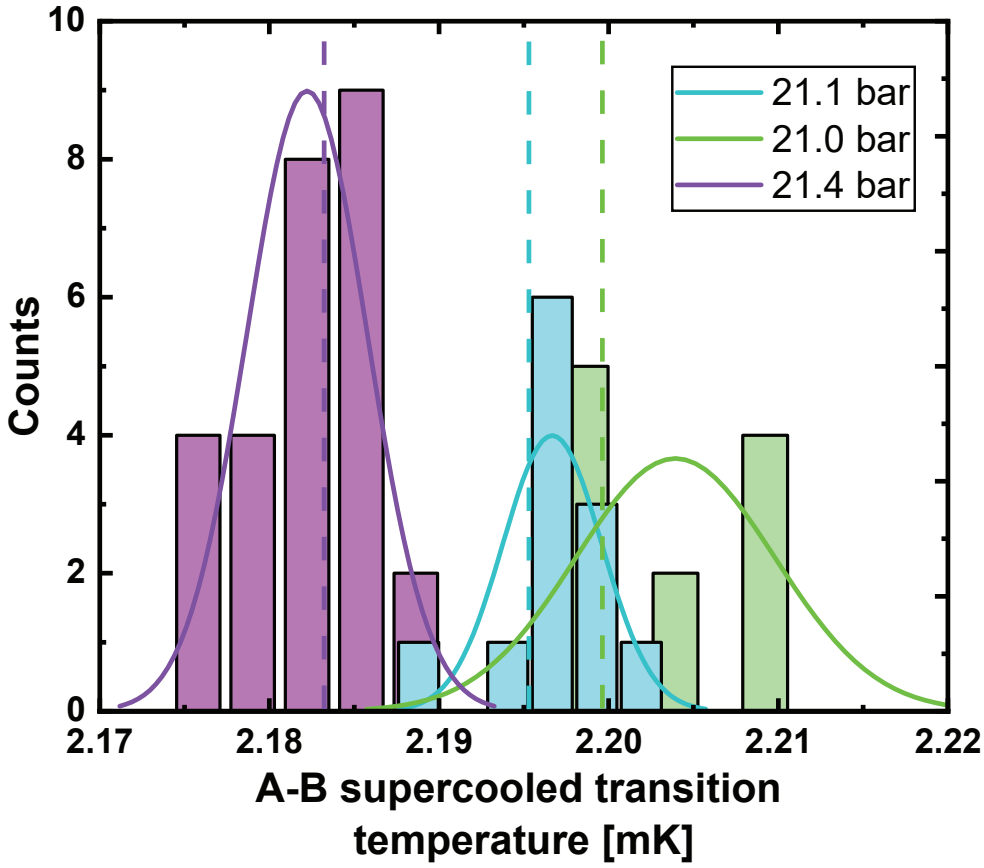

Supplementary Figure 4. The distribution of T_{AB} inferred from the Q of fast cooled transitions at the three lowest pressures where fast cooled transitions were reliably observed. At 21.4 bar (purple) the distribution has a $\sigma = 3.6$ μK, and 21.1 bar (cyan) $\sigma = 3.0$ μK, both centered at values close to the slow cooled T_{AB} shown as dashed lines. At 21.0 bar (green), the A$\rightarrow$B transitions were more broadly distributed.

We show the complete set of Q *vs* time at the 5 lowest pressures studied in Supplementary Figure 5. The A$\rightarrow$B transition under fast and slow cooling can readily be seen in the two highest pressure pulsed heating experiments and can be seen to be more widely distributed at 21.0 bar (see also Fig 3 b,c in the main paper). At 20.95 bar and 20.9 bar A$\rightarrow$B transitions can be seen under slow cooling but are not immediately evident under fast cooling.

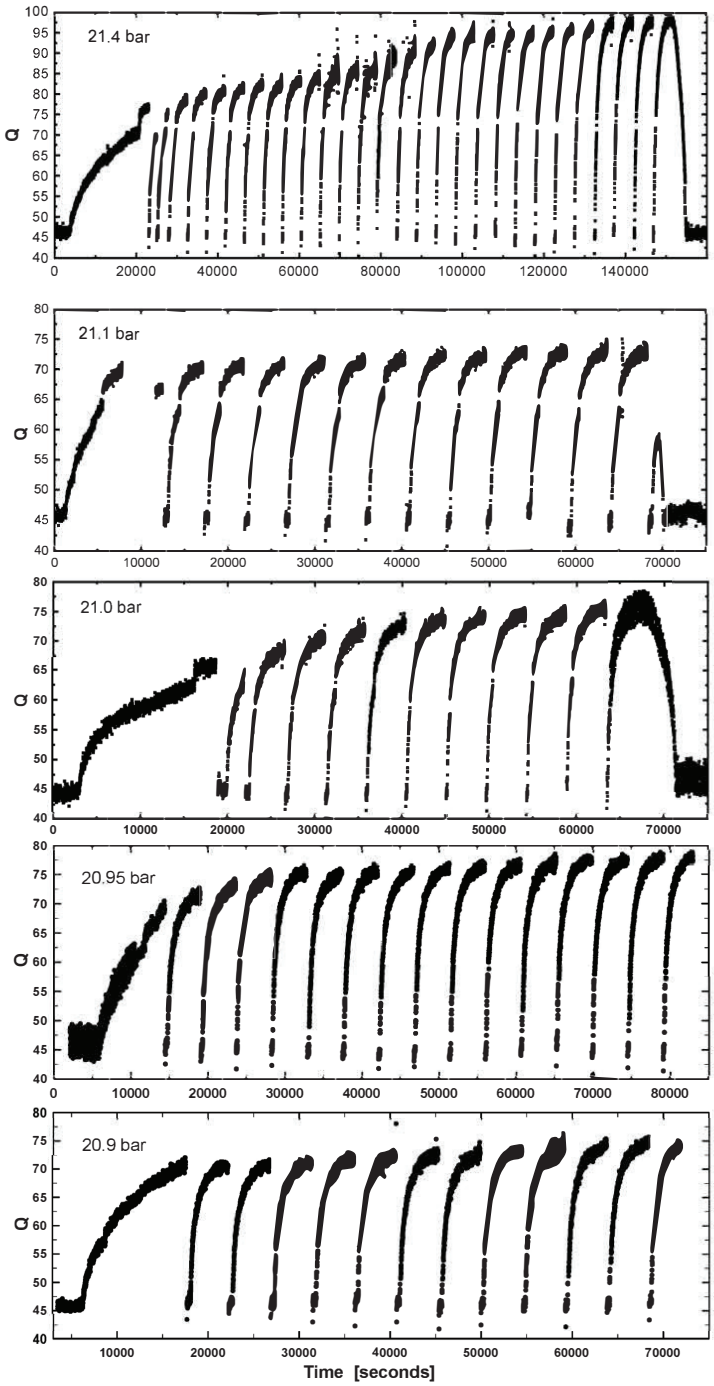

Supplementary Figure 5. Traces of the Q vs time for slow cooled transitions followed by a series of pulses at five different pressures 21.4 bar (top), 21.1 bar, 21.0 bar, 20.95 bar and 20.9 bar (bottom). The A→B transition can be seen as a gap in the Q *vs.* t traces and is well aligned with the slow cooled transition for the three highest pressures.

In analogy with Figures 3 b, c in Supplementary Figure 6 we show time shifted recoveries

following pulses at the two lowest pressures. In some recoveries A→B transitions can be seen and are marked with dashed lines. Other pulses appear to carry the IC directly to the B phase. The dotted line marks the location of the slow cooled transition.

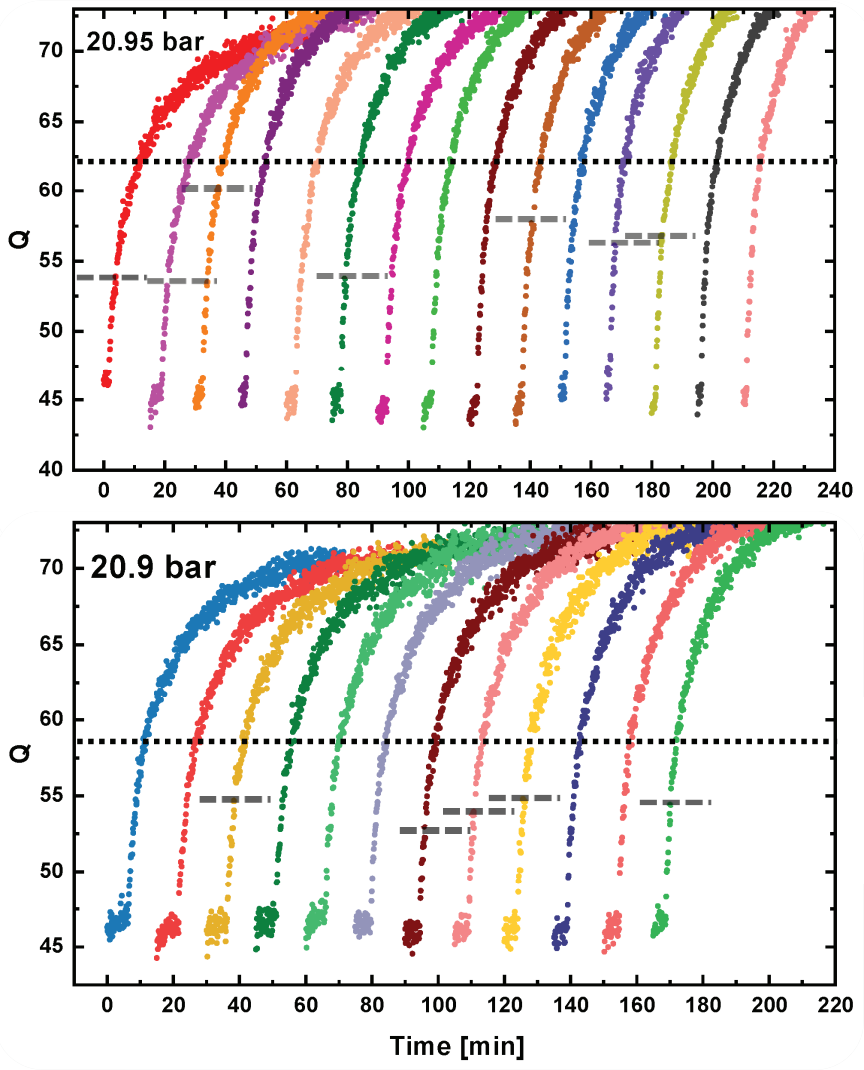

Supplementary Figure 6. Traces of the Q vs time of pulses at the two lowest pressures 20.95 bar (top) and 20.90 bar (bottom) after time shifting. The locations of the slow cooled A→B transition are shown by dotted lines. Poorly defined candidate A→B transitions following pulsed heating are marked by dashed lines. (See also Figure 3 b, c in the main paper).

In Supplementary Figure 7 we show the supercooled transitions seen in the heat exchange chamber (HEC). They show less supercooling than the IC presumably due to the sinter. Also shown are the data obtained by Kleinberg *et al.* [1] (see also Supplementary Figure 1).

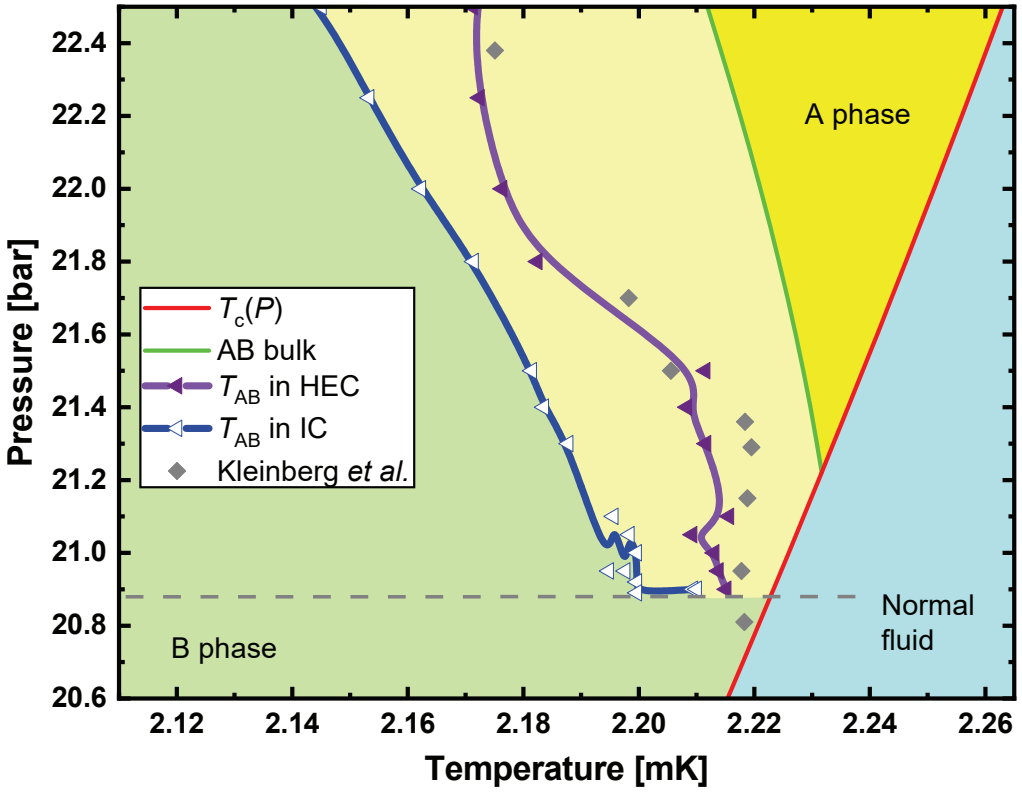

Supplementary Figure 7. The purple left pointing triangles and heavy purple line (guide to the eye) mark the position of the supercooled A→B transitions in the heat exchanger chamber (HEC) compared to the blue, left-pointing triangles and the heavy blue line that mark A→B transitions observed in the isolated chamber (IC). Together, they show the extent of supercooling of the A phase observed while cooling at constant pressure. The supercooling in the HEC is always observed to be less that that seen in the isolated chamber (IC). The red line shows the location of the second-order phase transition from the normal to the superfluid state ($T_c(P)$) and the green line shows the location of the equilibrium A-B transition ($T_{AB}(P)$). Grey diamonds mark the observed transitions shown in the experiments of Kleinberg *et al.* [1] in a cell where the ^{3}He liquid was in contact with powdered CMN (Cerous Magnesium Nitrate) refrigerant.

SUPPLEMENTARY NOTE 6. ANALOGY OF THE TERMINATION OF THE LINE OF CONSTANT PRESSURE COOLED A→B TRANSITIONS WITH A CLASSICAL CRITICAL POINT.

In Figures 3, 4 and 5 of the main paper (and in the text), we see that the line of constant pressure supercooled A→B transitions terminates away from T_c in analogy with the critical point in classical gas-liquid transitions. However, there are significant differences. Unlike the classical liquid-vapor transition (which is first order but not symmetry breaking), the A→B transition has a very small volume change and breaks symmetry. While cooling a classical system at constant pressure, supercooling involves conversion from the parent phase below the coexistence line (where the two phases have equal free energies). This supercooled region should be bounded by the coexistence line and a spinodal line defined by the divergence of the isothermal compressibility, or where an extremum point along an isotherm is attained[13]. The stability of the A phase at temperatures below the line of spinodal-like transitions is puzzling; spinodals designate where the metastable state becomes absolutely unstable. Thus we conclude that the $T_{A\to B}(P{=}\text{Const.})$ line cannot be a spinodal. However, the stability of the A phase below the $T_{A\to B}(P{=}\text{Const.})$ line represents a puzzle, because the free energy difference between the two phases is small. It may well be that the tensor and complex nature of the order parameter introduces an additional barrier or rigidity against the conversion from A→B.

It is possible that the extension of the supercooled A phase beyond the two-phase critical point may be related to echoes of the liquid-vapor coexistence line beyond the critical point (the "Widom Line"[14, 15] connecting fluid heat capacity maxima), but this remains speculative without detailed thermodynamic data. It seems much more likely that the transformation of the complex order parameter from the A to the B phase is the source of the path dependence and the stability of the A phase away from the line of constant pressure cooled A→B transitions.

SUPPLEMENTARY NOTE 7. INITIATION OF THE A-PHASE BELOW THE PCP.

The initiation of the A phase after crossing T_c below the polycritical point (despite the B phase's stability in this P, T) is worth discussion. A small magnetic field would insert an infinitesimal width of A phase between the normal state and the B phase [1, 16]. However, we see no B→A transition on warming assuring us that the magnetic field is indeed negligible. Our constant-pressure cooled data below the polycritical point bears resemblance to the data in 0.5 mT of Kleinberg [1] (Supplementary Figure 7). Another mechanism to nucleate the A phase in the IC below 22.22 bar references Cahn-Hilliard [17]. Since the channel that cools the ^{3}He in the IC is in the A phase, the surface-energy cost to grow a seed of the B phase in the IC just below T_c from the A phase filled channel exceeds the volume free-energy cost of the A over the B phase. Thus it is likely that the channel "seeds" the IC with the A phase. Once the A phase occupies the IC, B phase nucleation requires overcoming a barrier and leads to supercooling. We note that in Supplementary Figure 7, the A phase is seen to nucleate in the HEC and also in the experiments carried out in the presence of powdered CMN refrigerant [1]. The pores in the sintered powder and refrigerant also promote the A phase in the HEC volume while cooling.

SUPPLEMENTARY NOTE 8. LOBSTER POTS.

Yip and Leggett introduced the concept of a "lobster pot" (See Fig. 1 in [18]), a surface cavity connected to the bulk through an orifice. T_c in the cavity is suppressed relative to the bulk, and T_c in the orifice is further reduced. In this model, the cavity transitions from the normal state to the equilibrium phase at the reduced cavity T_c, encoding the memory of the P, T coordinates of T_c. When the orifice connecting the "lobster pot" to the bulk undergoes T_c, the memory stored in the lobster-pot is imprinted on the bulk. Thus, if the fluid in the IC is cooled through T_c at a high pressure, a "lobster-pot"is filled with A phase. When cooled through T_c near or below the polycritical pressure, the cavity fills with B phase, thus retaining memory of the pressure when it was cooled through T_c. A high pressure cooled experiment should supercool further because an A-phase filled cavity cannot provide a B phase "seed" to nucleate A→B. However, this model requires a very specific distribution of

cavities and orifices. For example, to achieve a cavity T_c reduction of 1% requires cavity radii ~ 1 μm[19, 20], and similar sized pores. Such pore-cavity combinations would favor the A phase even at low pressure, rendering the model problematic.

---

[1] R. L. Kleinberg, D. N. Paulson, R. A. Webb, and J. C. Wheatley, J. Low Temp. Phys. **17**, 521 (1974).

[2] P. J. Hakonen, M. Krusius, M. M. Salomaa, and J. T. Simola, Phys. Rev. Lett. **54**, 245 (1985).

[3] H. Fukuyama, H. Ishimoto, T. Tazaki, and S. Ogawa, Phys. Rev. B **36**, 8921 (1987).

[4] G. W. Swift and D. S. Buchanan, Jpn. J. Appl. Phys. **26**, 1828 (1987).

[5] P. Schiffer, M. T. O'Keefe, M. D. Hildreth, H. Fukuyama, and D. D. Osheroff, Phys. Rev. Lett. **69**, 120 (1992).

[6] D. Greywall, Phys. Rev. B **33**, 7520 (1986).

[7] R. Rusby, B. Fellmuth, J. Engert, W. Fogle, E. Adams, L. Pitre, and M. Durieux, J. Low Temp. Phys. **149**, 156 (2007).

[8] N. Zhelev, T. S. Abhilash, R. G. Bennett, E. N. Smith, B. Ilic, J. M. Parpia, L. V. Levitin, X. Rojas, A. Casey, and J. Saunders, Rev. Sci. Instrum. **89**, 073902 (2018).

[9] D. Lotnyk, A. Eyal, N. Zhelev, T. S. Abhilash, E. N. Smith, M. Terilli, J. Wilson, E. Mueller, D. Einzel, J. Saunders, and J. M. Parpia, Nat. Commun. **11**, 4853 (2020).

[10] J. M. Parpia, *The Viscosity of Normal and Superfluid Helium Three*, Ph.D. thesis, Cornell University (1979).

[11] J. M. Parpia and J. D. Reppy, Phys. Rev. Lett. **43**, 1332 (1979).

[12] K. Andres and W. Sprenger, Proceedings of LT14, Matti Krusius and Matti Vuorio, eds., **1**, 123 (1976).

[13] P. G. Debenedetti, Metastable liquids *concepts and principles* (Princeton University Press, Princeton, N.J., 1996) Chap. 2,3, pp. 63–233.

[14] L. Xu, P. Kumar, S. V. Buldyrev, S.-H. Chen, P. H. Poole, F. Sciortino, and H. E. Stanley, Proc. Natl. Acad. Sci. U.S.A. **102**, 16558 (2005).

[15] P. Schienbein and D. Marx, Phys. Rev. E **98**, 022104 (2018).

[16] D. N. Paulson, H. Kojima, and J. C. Wheatley, Phys. Rev. Lett. **32**, 1098 (1974).

[17] J. W. Cahn and J. E. Hilliard, J. Chem. Phys. **28**, 258 (1958).

[18] A. J. Leggett and S. K. Yip, in *Helium Three*, Modern Problems in Condensed Matter Sciences No. 26, edited by L. P. Pitaevskii and W. P. Halperin (Elsevier, Amsterdam, 1990) 3rd ed., Chapt. 8, pp. 523–707.

[19] L. H. Kjäldman, J. Kurkijärvi, and D. Rainer, J. Low Temp. Phys. **33**, 577 (1978).

[20] V. Kotsubo, K. D. Hahn, and J. M. Parpia, Phys. Rev. Lett. **58**, 804 (1987).